Precise Control of InP Quantum Dot Growth via Recyclable Indium Adducts

Ashleigh J. Cartlidge,[a] Theodore A. Gazis,[a,b] Ufedo-ojo Pitas,[a] Jasmine E. Robertson,[a] Lauren Matthews,[c] Martin J. Hollamby[a] and Peter D. Matthews*[a]

a. School of Chemical & Physical Sciences, Keele University, Newcastle-under-Lyme, Staffordshire, ST5 5BG, UK.
b. Department of Chemistry, Materials, and Chemical Engineering "Giulio Natta", Politecnico di Milano, Piazza Leonardo da Vinci 32, IT-20133 Milano, Italy
c. ISIS Pulsed Neutron Source, Rutherford Appleton Laboratory, Didcot, OX11 0QX, (UK).

p.d.matthews@keele.ac.uk

Contents

1. General Experimental

All experiments were performed under an inert atmosphere of nitrogen, utilizing standard glovebox/Schlenk line procedures. All glassware was dried in an oven at 100 °C overnight prior to use. All chemicals were purchased from Fluorochem, the triarylphosphines and oleylamine were used without purification. Ethyl acetate was dried over 4Å sieves and indium trichloride was purified by dissolving in ethyl acetate, filtering to remove undissolved contaminants and then the solvent removed *in vacuo* before drying under dynamic vacuum at 80 °C for 18h.

UV-vis measurements were taken on a Varian Cary 50 Bio using a quartz cuvette. Approx 0.1 mL aliquots were removed from the reaction mixture using a needle and syringe and placed in an Eppendorf tube. 20 μL of this was removed using an autopipette and added to 2 mL of spectroscopic grade toluene in a quartz cuvette.

^{1}H, ^{31}P and ^{19}F NMR spectra were recorded on a Bruker Ascend 400 spectrometer. $^{31}P\{^{1}H\}$ spectra were acquired with 16 scans and a d1 = 80 s.

X-ray photoelectron spectroscopy (XPS) was performed using Al Kα X-rays (1.486 keV photon energy, 20 mA emission at 300 W) in an Axis Supra+ spectrometer (Kratos Analytical). The X-ray spot was approx. 1 mm diameter. Survey spectra were measured with pass energy 80 eV, and high-resolution core level spectra with 20 eV. Analysis was performed in CASAXPS. Binding energy positions are compared to literature values, including the online database from NIST, USA, https://dx.doi.org/10.18434/T4T88K . Charge neutralization of powders and insulators is achieved using a low energy electron source in vacuum (PREVAC). The measurements were performed under ultra-high vacuum conditions with an instrument base pressure of approx. $1x10^{-8}$ mbar. Binding energy calibration is performed using the C 1s peak (for graphitic carbon) at 284.8 eV for aliphatic / hydrocarbon. The sampling depth of XPS in InP (measuring the In 3d core level) is approx. 7 nm.

Elemental analysis was performed by the Elemental Analysis Services Team at London Metropolitan University using a ThermoFlash 2000.

The code used to analyse the data can be found at:
https://github.com/pm418chem/InP_QD_Analysis

2. Precursors

The synthesis of the triarylphosphine indium chloride adducts was adapted from literature procedures and carried out under air sensitive conditions.[1] All adducts were prepared by dissolving 1.74 mmol of $InCl_3$ in ethyl acetate (50 mL), and a stoichiometric amount of the phosphine ligands in the same solvent (3.48 mmol for the least sterically and 1.74 mmol for sterically demanding phosphine substituents). The resulting $InCl_3$ solution was added to the phosphine solution and left to stir at room temperature. During stirring, white powders of these adducts precipitated and were collected on a filter and dried *in vacuo*.

$(PPh_3)_2InCl_3$ (1)
Yield = 112 mg, 85%
Elemental analysis: Found: C57.6%, H3.8%; Calc for $C_{36}H_{30}Cl_3InP_2$: C58.0%, H4.0%

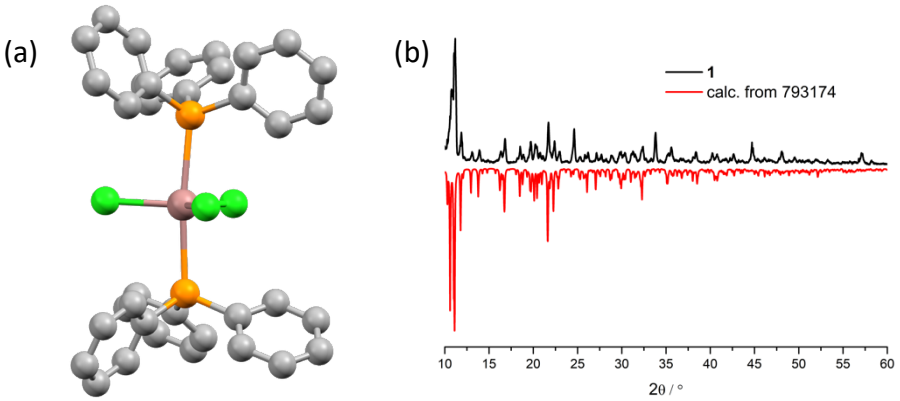

Fig S1. (a) Molecular structure of **1**, as reported by Chen et al., CCDC entry 793174.[1] Grey = C, green = Cl, brown = In, orange = P. H omitted for clarity. (b) PXRD pattern of **1** (black) showing good agreement with the calculated from the single crystal data (red).

$[P(4\text{-}MeOC_6H_5)_3]_2InCl_3$ (2)
Yield = 97 mg, 55%
Elemental analysis: Found: C53.9% H4.8%; Calc for C42H42Cl3InO6P2: C54.5%, H4.6%

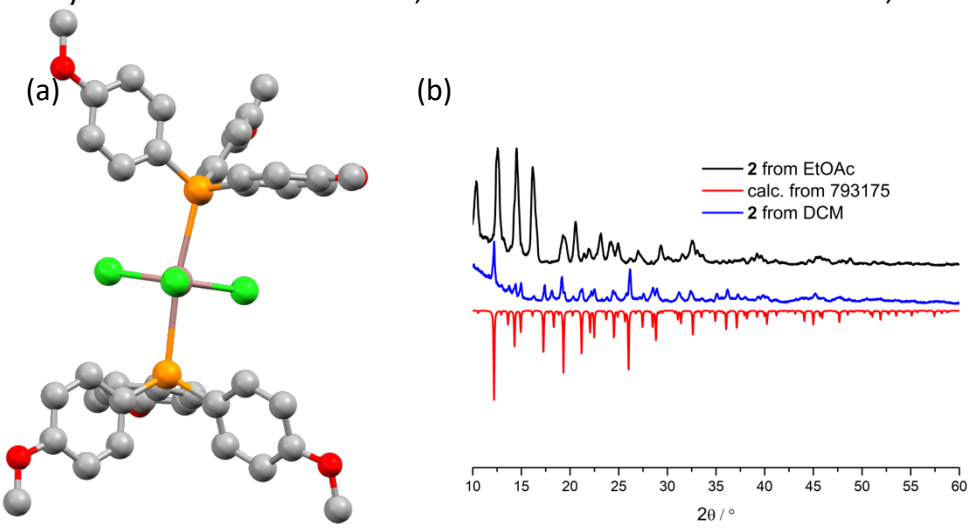

Fig S2. (a) Molecular structure of **2**, as reported by Chen et al., CCDC entry 793175.[1] Grey = C, red = O, green = Cl, brown = In, orange = P. H omitted for clarity. (b) PXRD pattern of as prepared from ethyl acetate **2** (black), and recrystalised from DCM (blue) showing good agreement with the calculated from the single crystal data (red). We have prepared

compound **2** by precipitating from ethyl acetate, which follows the literature procedure for making this.[1] The elemental analysis indicates clean formation of **2** with no co-crystallised solvent. The single crystal structure that we used to simulate the pattern was obtained by recrystallising from dichloromethane and includes some dichloromethane within it as a solvent of crystallisation. As our material does not contain solvent the PXRD pattern (black) will be different as the packing and thus cell parameters will be different. We have recrystallised compound **2** from DCM and obtained a PXRD pattern (blue) that matches that of the calculated one (red) .

$[P(4\text{-}FC_6H_4)_3]_2InCl_3$ (3)
Yield = 144 mg, 82%
Elemental analysis: Found: C50.4%5, H3.0% ; Calc for $C_{36}H_{24}Cl_3InF_6P_2$: C50.7%, H2.8%

$[P(2\text{-}MeOC_6H_4)_3]InCl_3$ (4)
Yield = 118 mg, 59%
Elemental analysis: Found: C43.7% H3.8%; Calc for $C_{21}H_{21}Cl_3InO_3P$: C44.0%, H3.7%

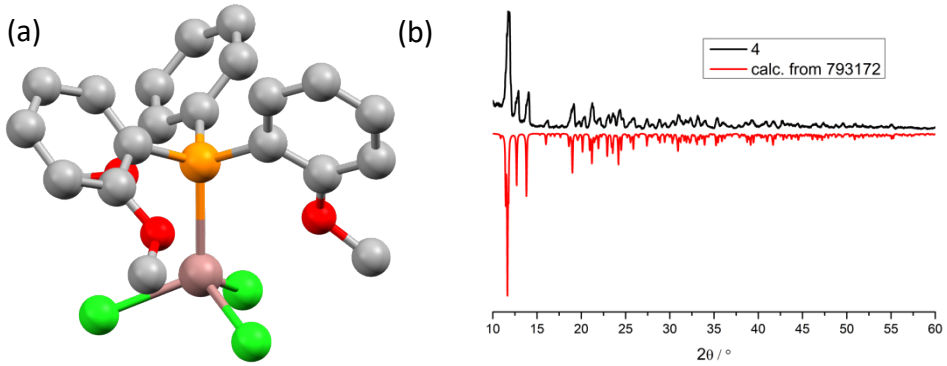

Fig S3. (a) Molecular structure of **4**, as reported by Chen et al., CCDC entry 793172.[1] Grey = C, red = O, green = Cl, brown = In, orange = P. H omitted for clarity. (b) PXRD pattern of **4** (black) showing good agreement with the calculated from the single crystal data (red).

Table S1. Precursor Properties. Structural information obtained from CCDC entries 793172, 793174, 793175.[1] The crystal structure of **3** has not been reported.

Precursor	**In-Cl bond length / Å**	**In-P bond length / Å**	**Phosphine pKa**[2]	**Cone angle / °** From Ref [3]
$InCl_3$	2.30[4]	-	-	-
$(PPh_3)_2InCl_3$ (**1**)	2.391-2.405	2.868	2.73	145
$[P(4\text{-}MeOC_6H_5)_3]_2InCl_3$ (**2**)	2.393-2.405	2.697-2.729	4.57	145
$[P(4\text{-}FC_6H_4)_3]_2InCl_3$ (**3**)	-	-	1.97	145
$[P(2\text{-}MeOC_6H_4)_3]InCl_3$ (**4**)	2.377-2.382	2.543	-	176

3. UV-vis spectra

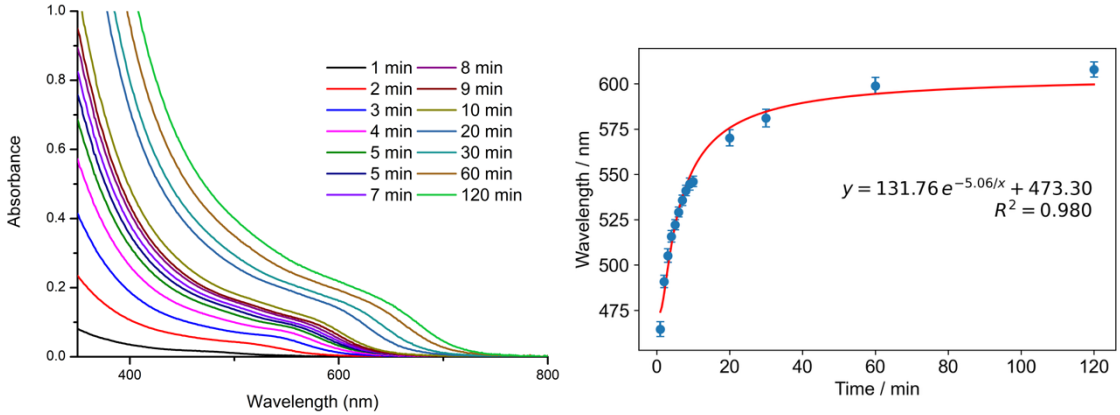

Figure S4. (a) UV-vis spectra monitoring the growth of InP and (b) change in the lowest energy excitonic transition (LEET) over the course of the reaction when using $InCl_3$ as the indium source.

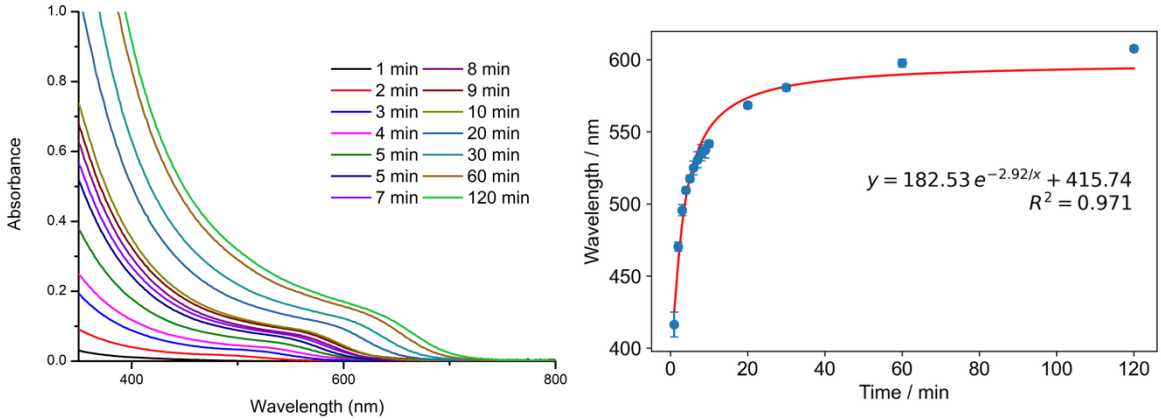

Figure S5. (a) UV-vis spectra monitoring the growth of InP and (b) change in the lowest energy excitonic transition (LEET) over the course of the reaction when using **1** as the indium source.

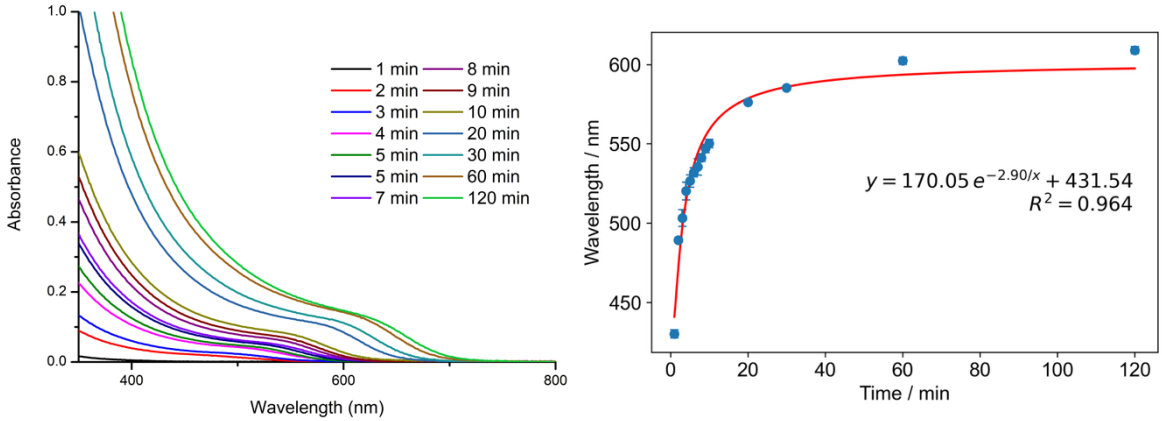

Figure S6. (a) UV-vis spectra monitoring the growth of InP and (b) change in the lowest energy excitonic transition (LEET) over the course of the reaction when using **2** as the indium source.

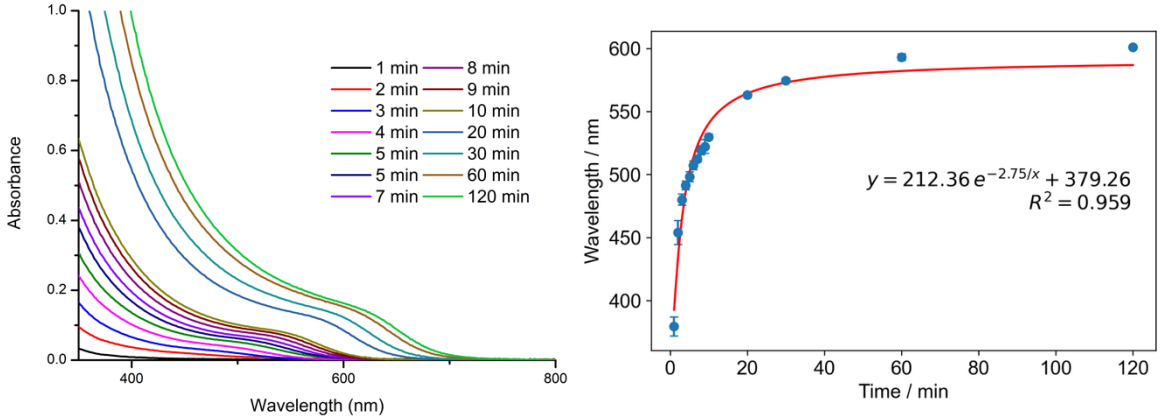

Figure S7. (a) UV-vis spectra monitoring the growth of InP and (b) change in the lowest energy excitonic transition (LEET) over the course of the reaction when using **3** as the indium source.

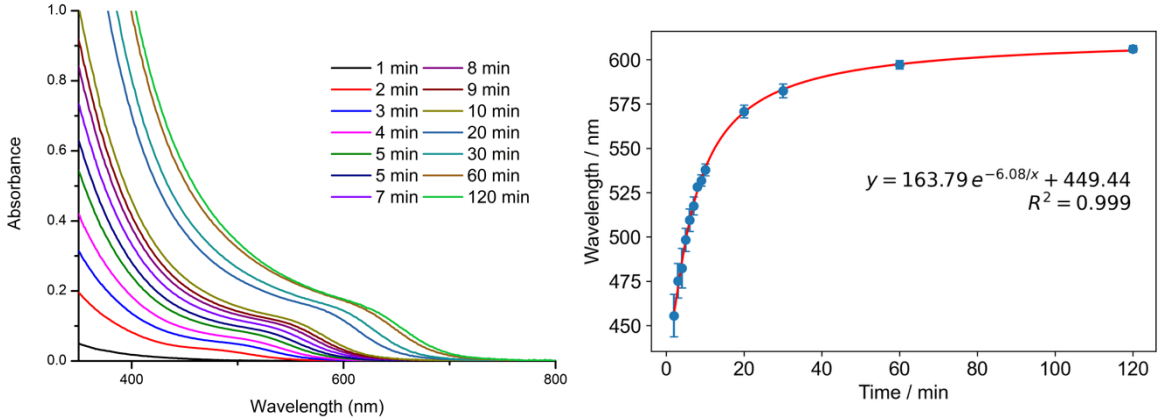

Figure S8. (a) UV-vis spectra monitoring the growth of InP and (b) change in the lowest energy excitonic transition (LEET) over the course of the reaction when using **4** as the indium source.

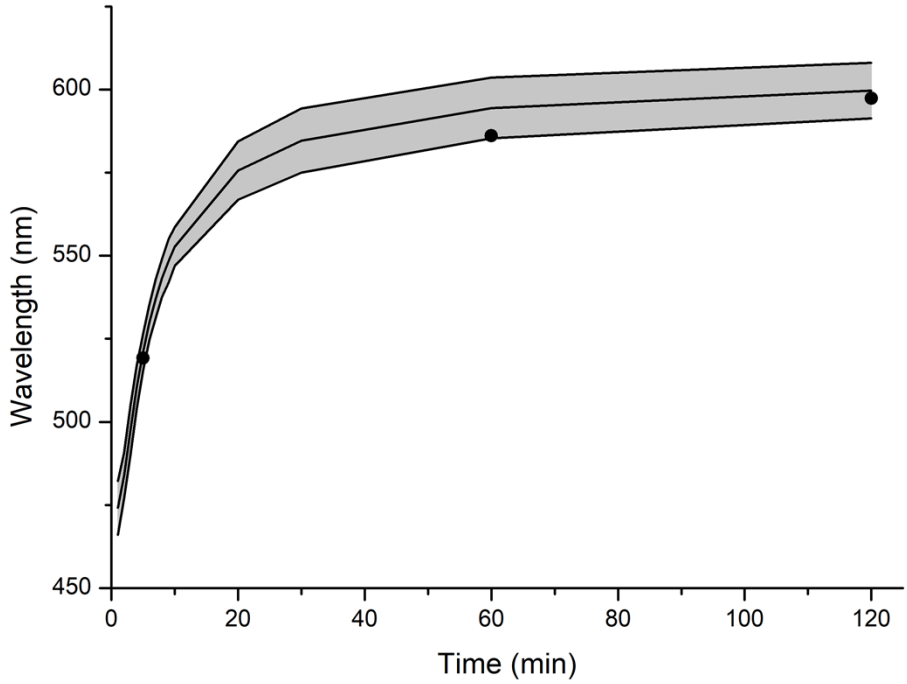

Figure S9. Predicted LEET absorbance (black line) with a two standard error range marked on (grey area) and obtained LEETs (black circles) for $InCl_3$ as indium source.

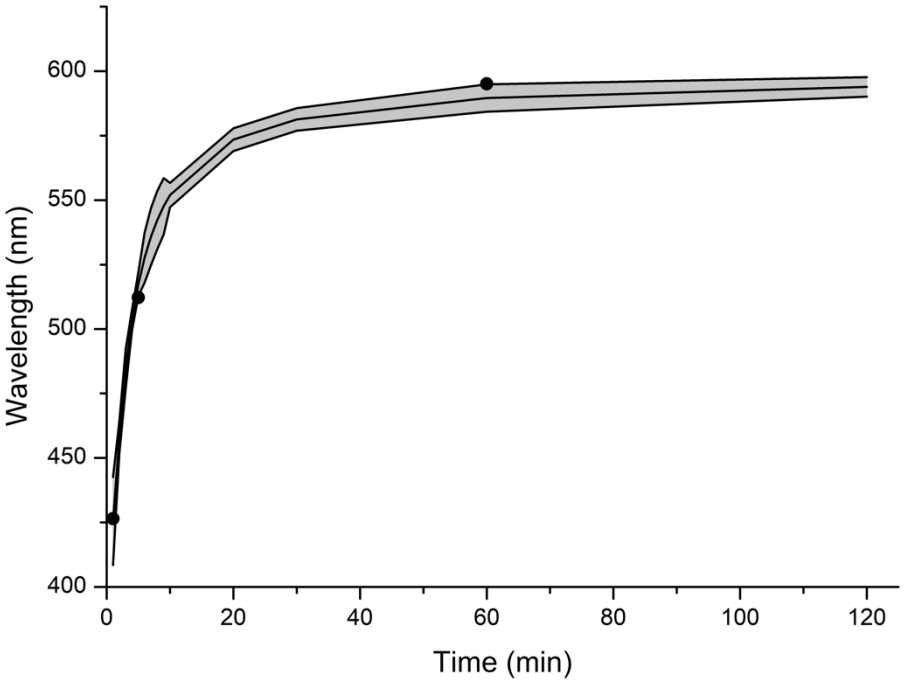

Figure S10. Predicted LEET absorbance (black line) with a two standard error range marked on (grey area) and obtained LEETs (black circles) for **1** as indium source.

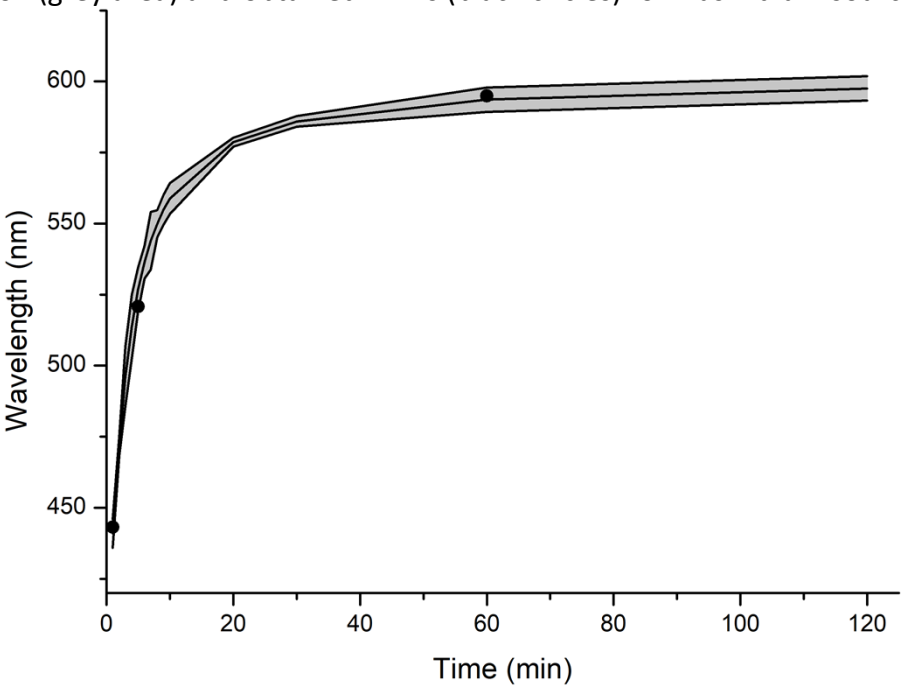

Figure S11. Predicted LEET absorbance (black line) with a two standard error range marked on (grey area) and obtained LEETs (black circles) for **2** as indium source.

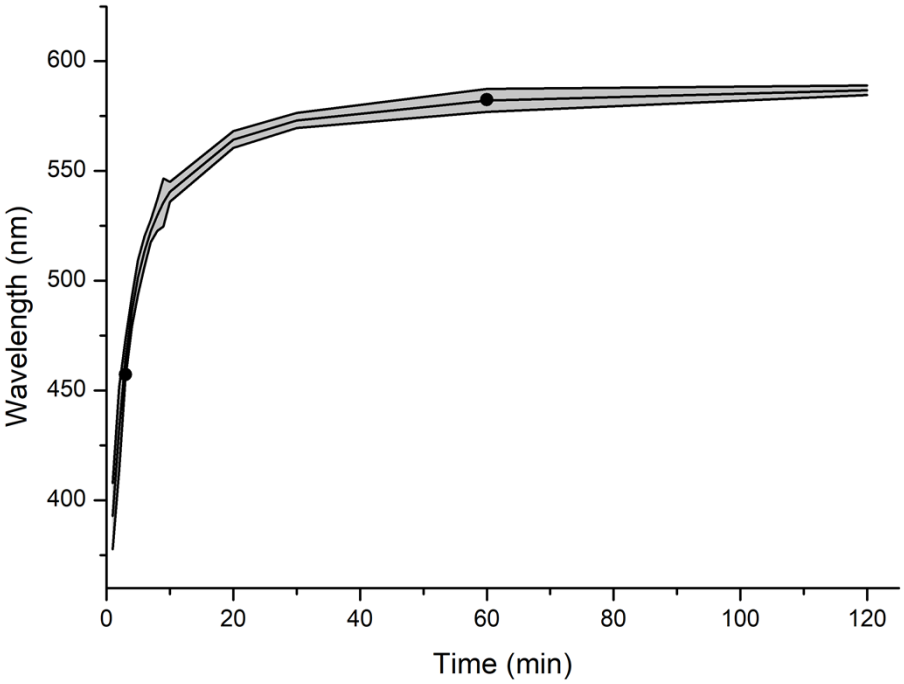

Figure S12. Predicted LEET absorbance (black line) with a two standard error range marked on (grey area) and obtained LEETs (black circles) for **3** as indium source.

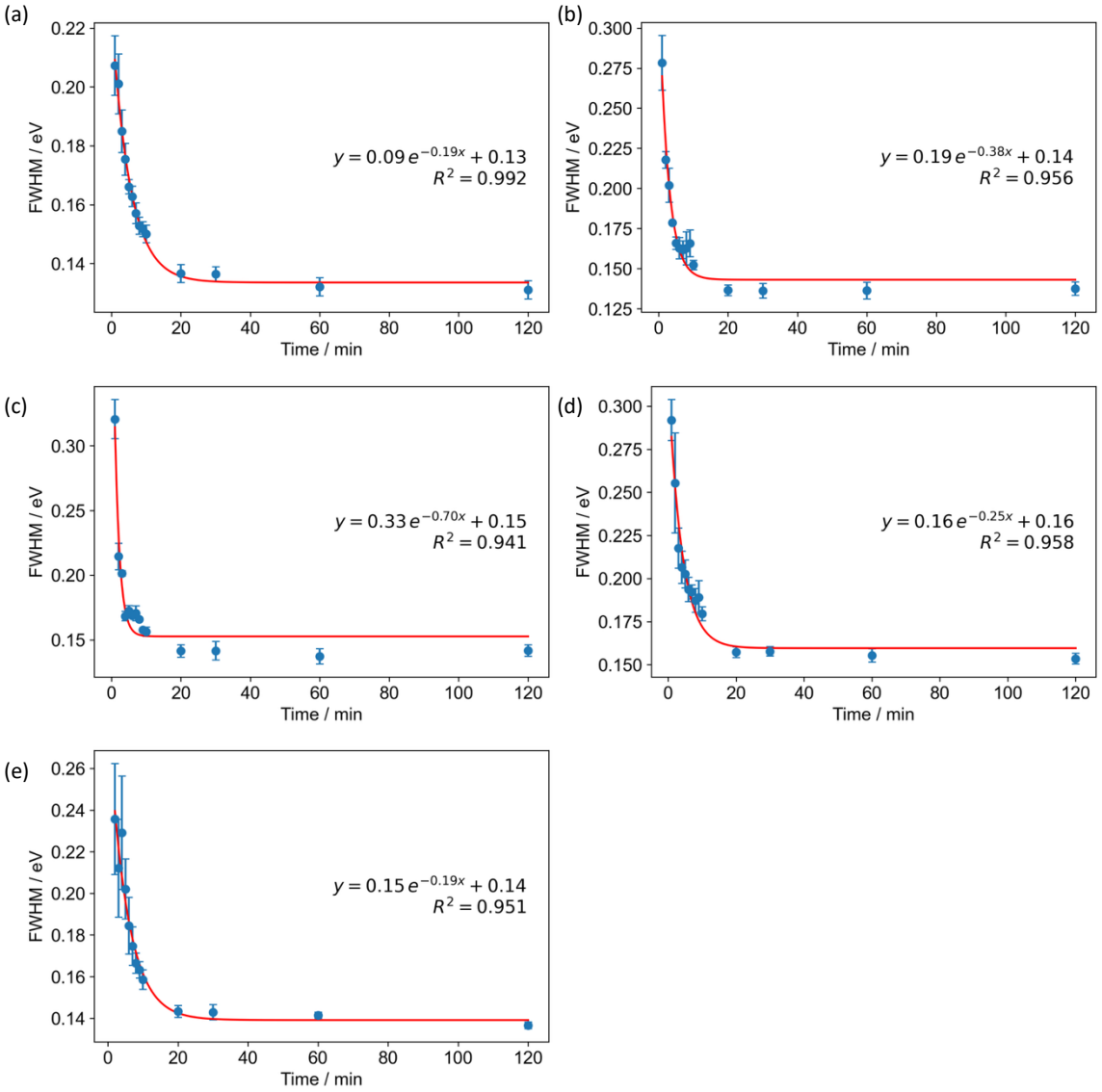

Figure S13. Progression of full width half maxima (FWHM) over the course of the reaction for InP QD syntheses using: (a) $InCl_3$, (b) **1**, (c) **2**, (d) **3** and (e) **4** as the indium source.

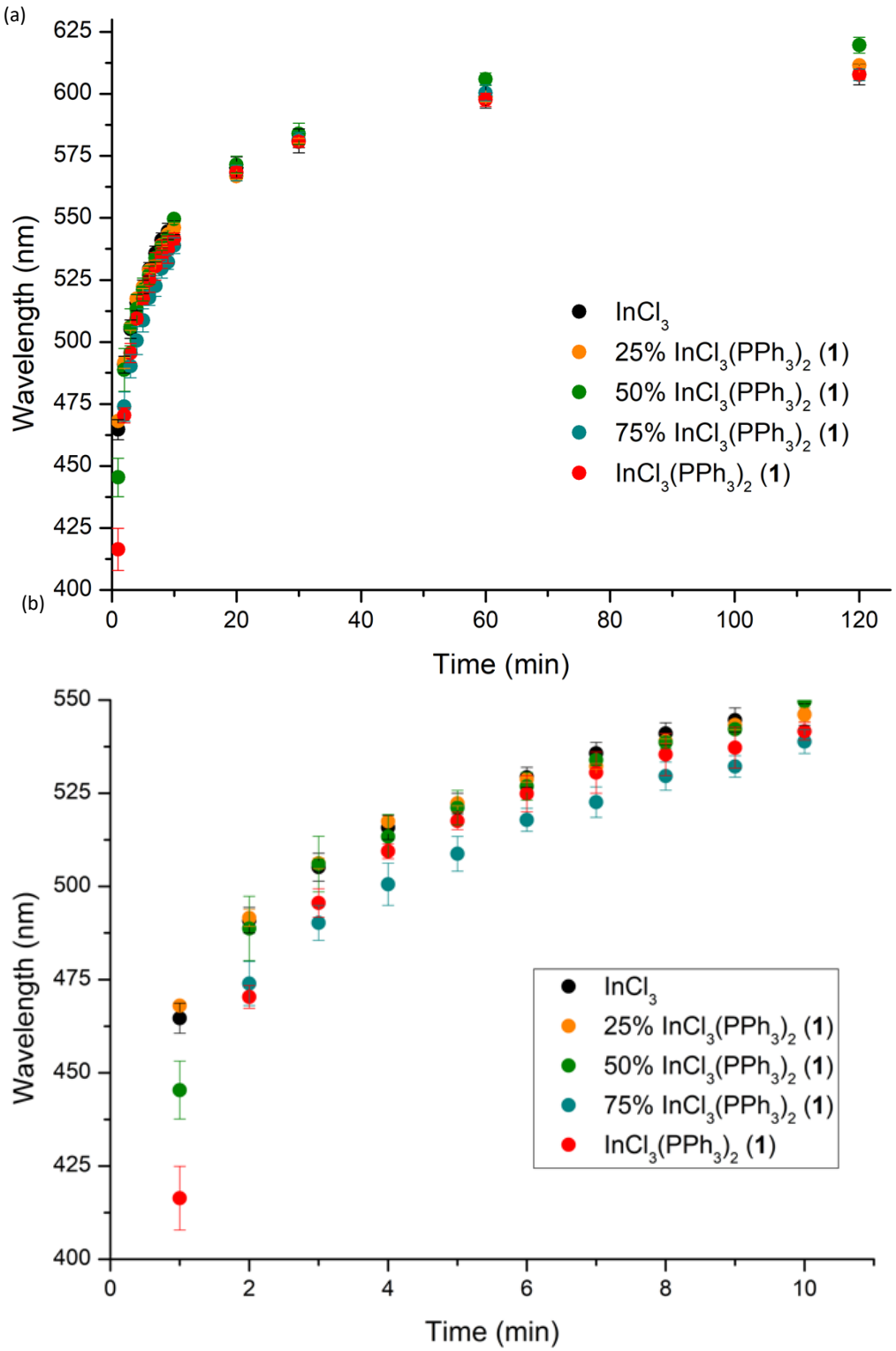

Figure S14. Change in the lowest energy excitonic transition (LEET) over (a) the course of the reaction and (b) the first 10 mins, when using various ratios of $InCl_3$: **1** as the indium source.

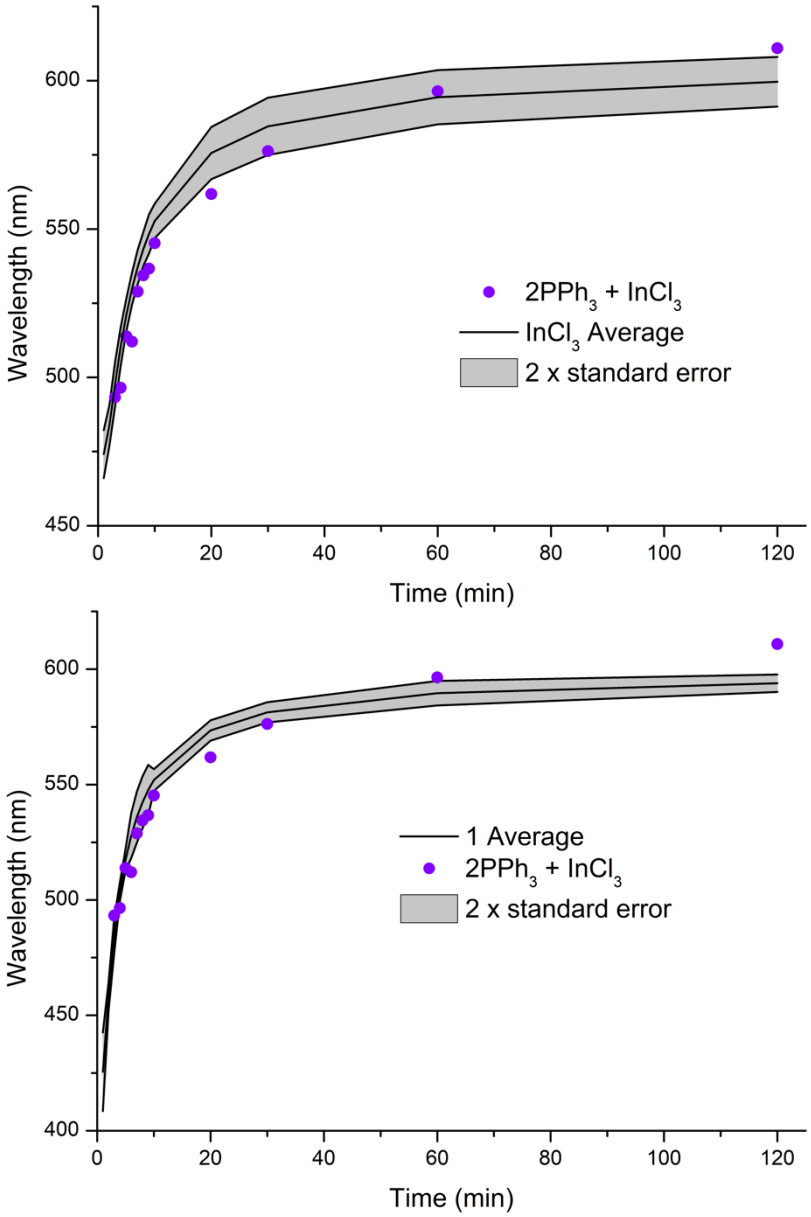

Figure S15. Predicted LEET absorbance (black line) with a two standard error range marked on (grey area) for (a) $InCl_3$ and (b) **1** as indium source with measurements from a mixture of $2PPh_3$ and $InCl_3$ as the indium source (purple circles).

4. NMR Spectra

Figure S16. $^{31}P\{^{1}H\}$ NMR spectra of a reaction mixture aliquot (top) and purified InP QD made with **3** (bottom), with the purified spectra showing no coordinated $P(C_6H_5F)_3$ (-9 ppm)

Figure S17. ^{19}F NMR spectra of a reaction mixture aliquot (top) and purified InP QD made with **3** (bottom), with the purified spectra showing no coordinated $P(C_6H_5F)_3$ (-111 ppm)

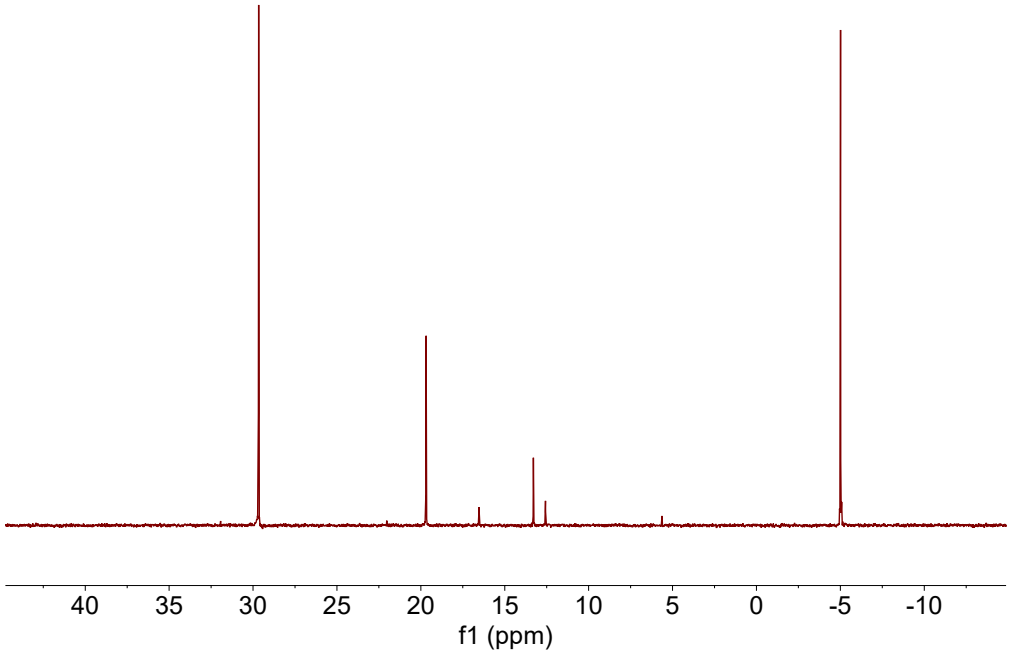

Figure S18. $^{31}P\{^{1}H\}$ NMR spectra of the first supernatant from the purification of an InP QD made with **1**, indicating large amounts of free PPh_3 (-6 ppm). Key peaks: phosphonium salt by-product (30.0 ppm), phosphonium oxide species from purification work-up (20 ppm), aminophosphine tautomers (12-13 ppm) and PPh_3 (-5.3 ppm).

Figure S19 $^{31}P\{^{1}H\}$ NMR spectra of a reaction using **3**, demonstrating a growth of $P(C_6H_5F)_3$ over time.

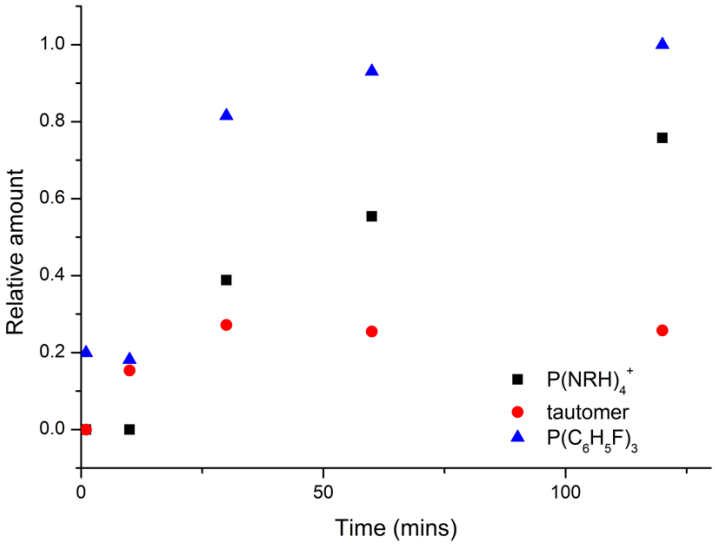

Figure S20. Relative ratios of the key components in a reaction using **3**, determined from $^{31}P\{^{1}H\}$ NMR spectra using an internal standard of trioctylphosphine. A 50 μL aliquot of reaction mixture was added to 0.6 mL of C_6D_6 and spiked with 20 μL of trioctylphosphine. A J Youngs NMR tube was used to ensure air sensitivity.

5. Determination of LEET

For all spectra an absorbance tail could be identified, and this was converted to eV and fitted to a Gaussian of the form:

$$f(x,\sigma) = B + Aexp^{\frac{-(x_0 - x^2)}{2\sigma^2}}$$

Where B is equal to the energy of absorbance at 1.55 eV (which is assumed to have no contribution from the nanoparticles), A is equal to the absorbance of the lowest energy electronic transition, 2σ is the full width at half maximum (FWHM) of the tail, and x_0 is the energy of the lowest energy electronic transition.[5]

6. InP concentration and Initial InP Growth Rate Calculations

The concentration of InP in the reaction mixture was calculated using previously established techniques.[6–8] This makes the assumption that all absorbance at 413 nm can be linked to InP nanocrystals through the following equation:

$$n_{cuvette} = \frac{A\ ln10}{\mu_{i,th}\ L} \times \frac{V_{cuvette}}{V_{mol}}$$

Where $n_{cuvette}$= number of moles of InP in the cuvette, A = the absorbance at 413 nm, $\mu_{i,th}$= theoretical intrinsic absorption coefficient (8.5×10^6 m^{-1} in toluene), *L* = path length, $V_{cuvette}$ = volume of the cuvette and V_{mol} = molar volume of InP (3.0×10^{-5} $m^3\ mol^{-1}$).

In order to take consistent UV-vis spectroscopy measurements, we took 20 µL reaction aliquots dissolved in 2.00 mL of toluene in the cuvette.

The initial reaction rates were determined by calculating the change in concentration of InP over a short period of time.

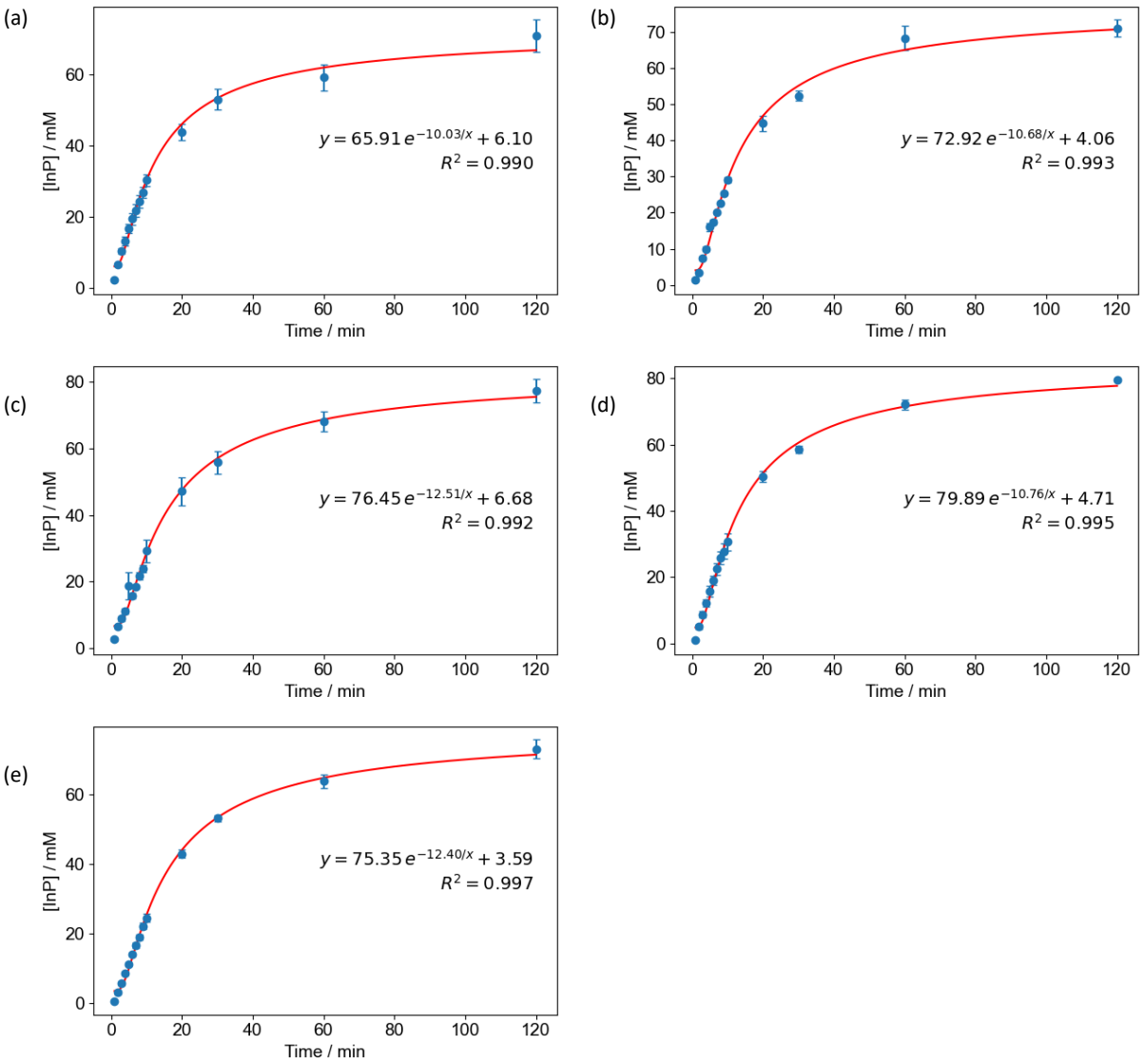

Figure S21. Progression of [InP] over the course of the reaction for InP QD syntheses using: (a) $InCl_3$, (b) **1**, (c) **2**, (d) **3** and (e) **4** as the indium source.

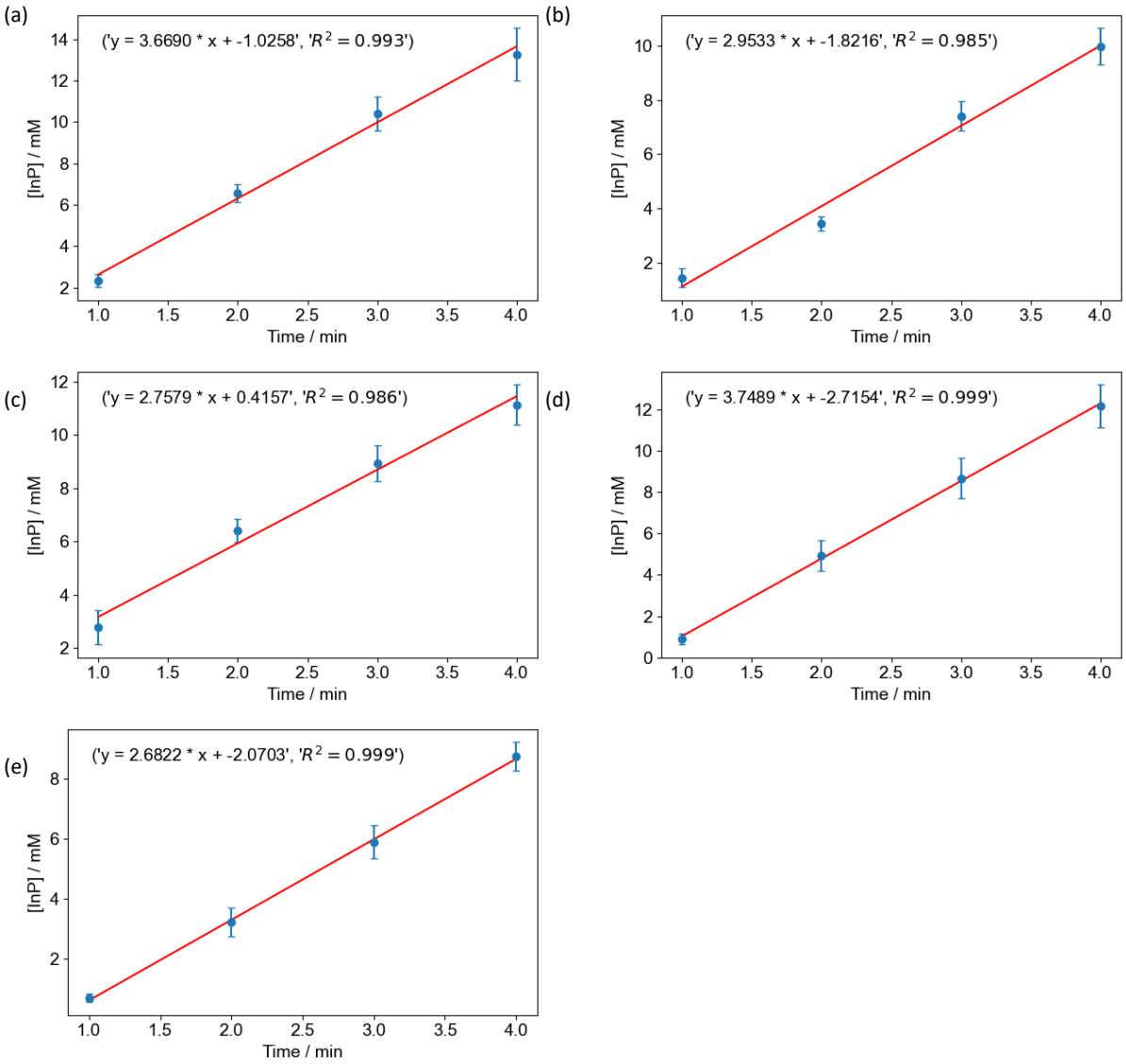

Figure S22. Progression of [InP] over the course of the reaction for InP QD syntheses for the first 4 minutes, fitted to a straightline using: (a) $InCl_3$, (b) **1**, (c) **2**, (d) **3** and (e) **4** as the indium source.

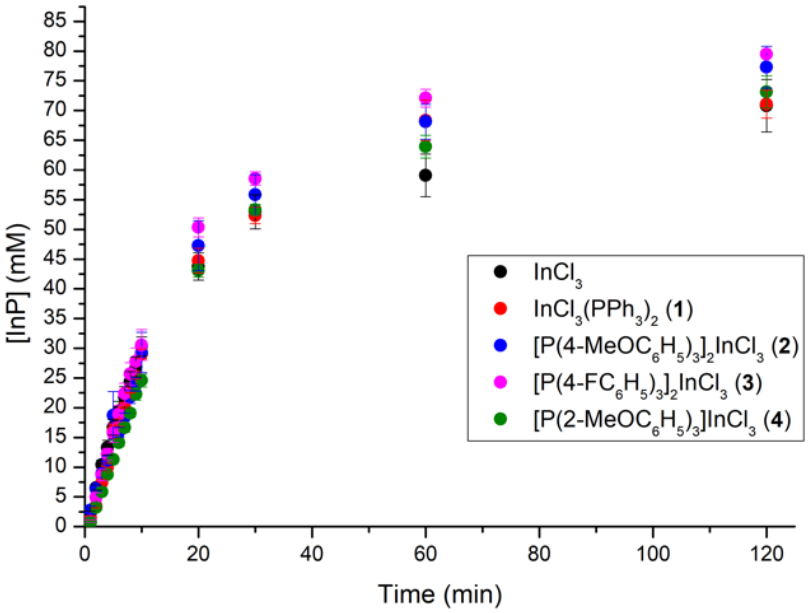

Figure S23. Progression of [InP] over the course of the reaction using $InCl_3$ (black), $(Ph_3P)_2InCl_3$ (**1**, red), $[P(4\text{-}MeOC_6H_5)_3]_2InCl_3$ (**2**, blue), $[P(4\text{-}FC_6H_4)_3]_2InCl_3$ (**3**, pink) and $[P(2\text{-}MeOC_6H_4)_3]InCl_3$ (**4**, green) as the indium source.

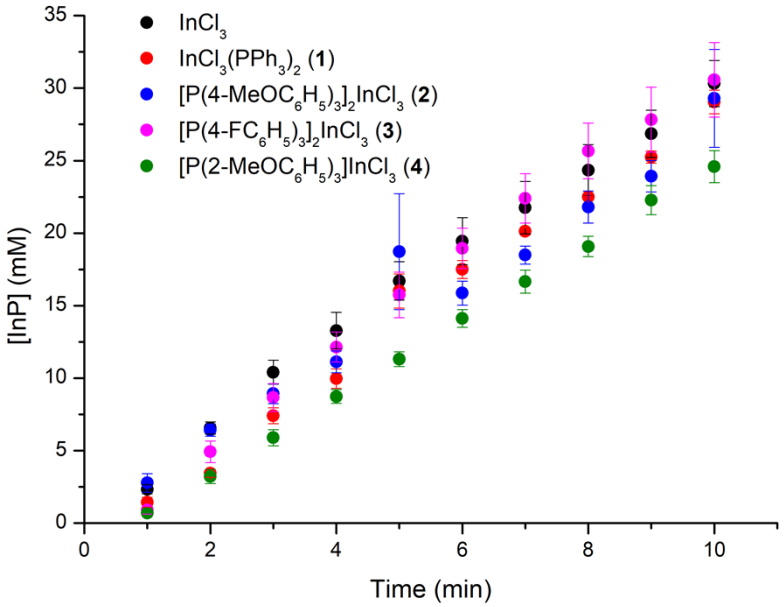

Figure S24. Progression of [InP] over the first 10 minutes of the reaction using $InCl_3$ (black), $(Ph_3P)_2InCl_3$ (**1**, red), $[P(4\text{-}MeOC_6H_5)_3]_2InCl_3$ (**2**, blue), $[P(4\text{-}FC_6H_4)_3]_2InCl_3$ (**3**, pink) and $[P(2\text{-}MeOC_6H_4)_3]InCl_3$ (**4**, green) as the indium source.

Table S2. Initial rates of InP formation, measured over the first 10 minutes of the reaction from the [InP].

Indium Source	**Initial rate / mM min^{-1}**
100% $InCl_3$	3.67
25% $(PPh_3)_2InCl_3$ (**1**) : 75% $InCl_3$	3.66
50% $(PPh_3)_2InCl_3$ (**1**) : 50% $InCl_3$	2.95
75% $(PPh_3)_2InCl_3$ (**1**) : 25% $InCl_3$	2.84
100% $(PPh_3)_2InCl_3$ (**1**)	2.95

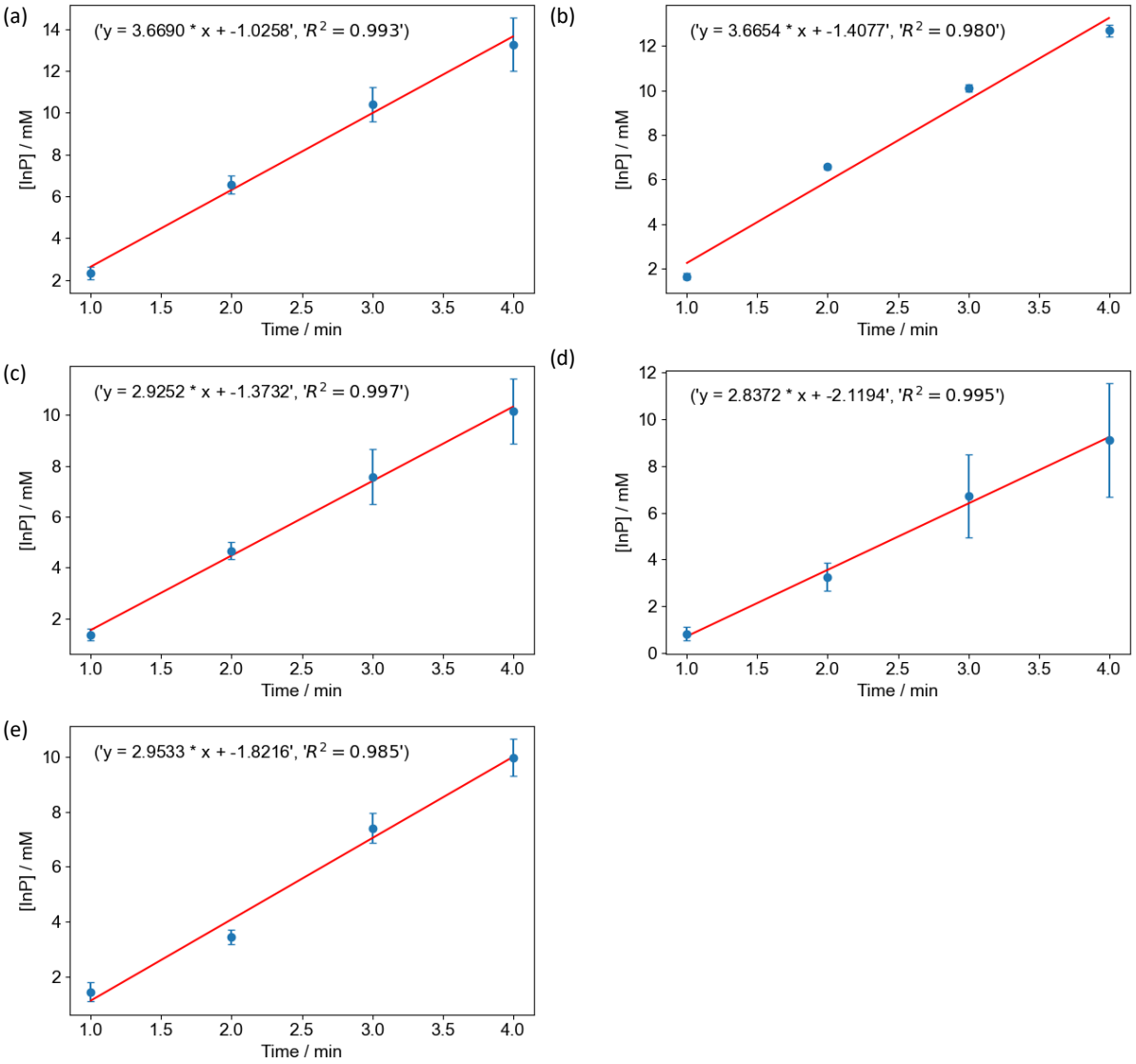

Figure S25. Progression of [InP] over the course of the reaction for InP QD syntheses for the first 4 minutes, fitted to a straightline using: (a) 100% $InCl_3$, (b) 25% **1** : 75% $InCl_3$, (c) 50% **1** : 50% $InCl_3$, (d) 75% **1** : 25% $InCl_3$ and (e) 100% **1** as the indium source.

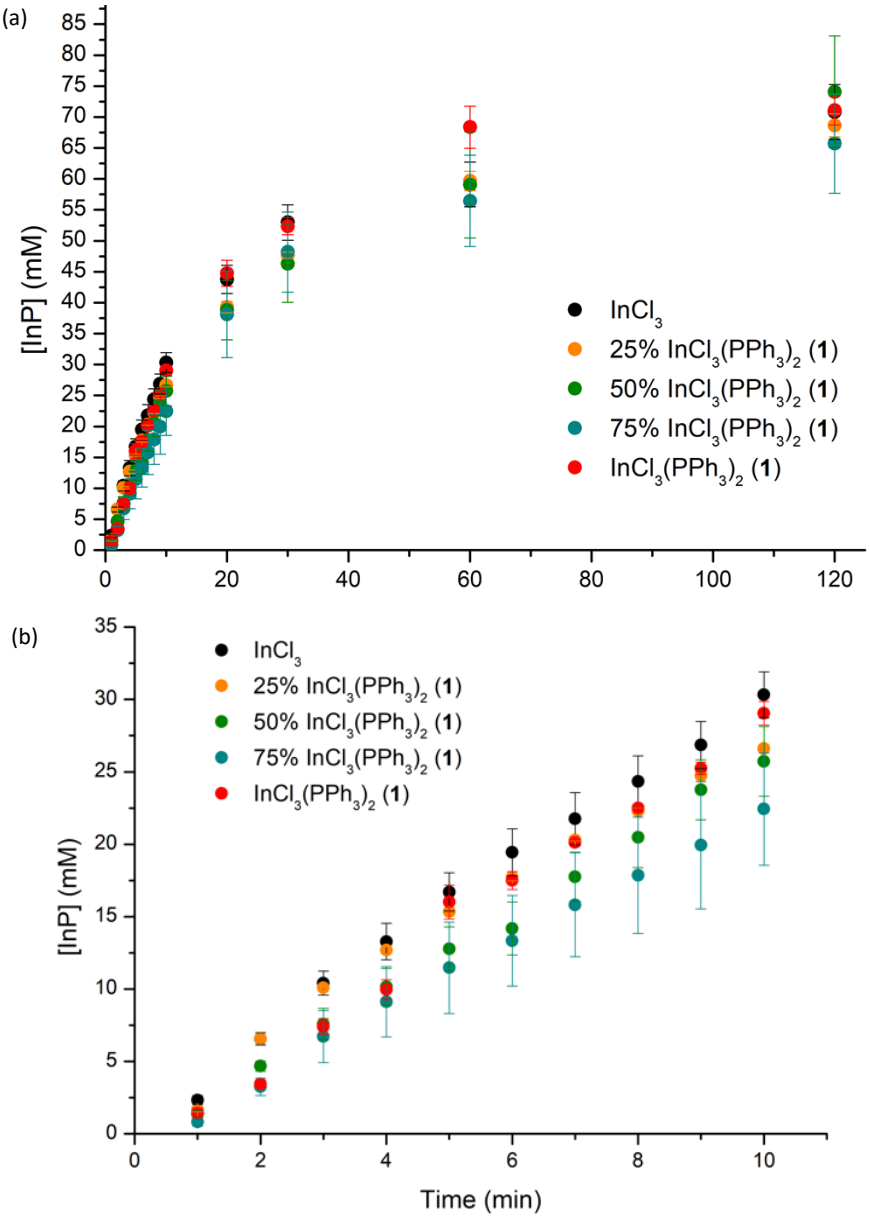

Figure S26. Progression of [InP] over the course of the reaction using ratios of **1** : $InCl_3$ over the course of (a) the whole reaction and (b) the first 10 minutes.

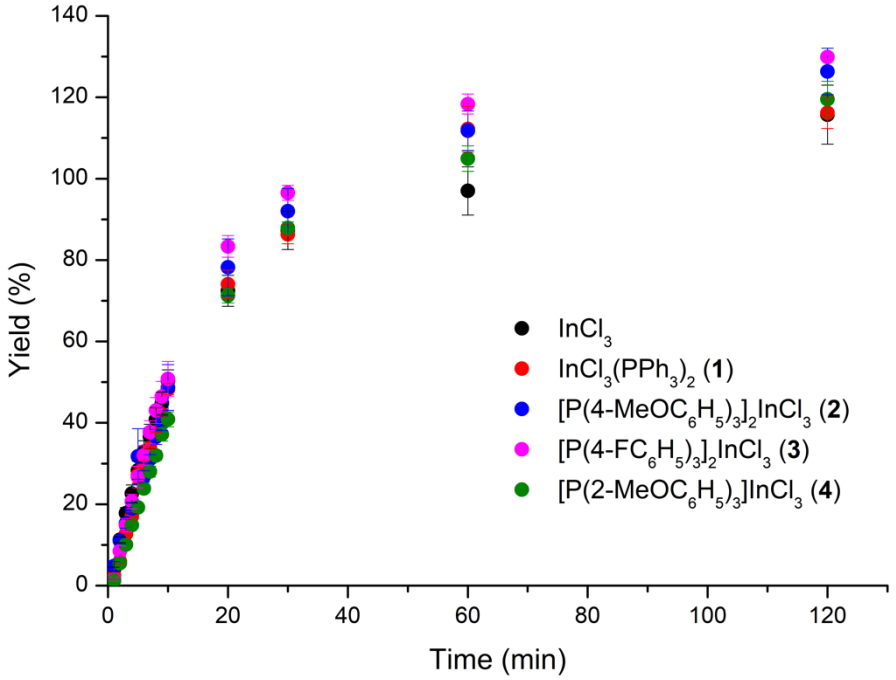

Figure S27. InP yield obtained using $InCl_3$ and precursors **1**-**4**. The yield was calculated by dividing the moles of InP units in the reaction flask by the theoretical maximum moles of InP (0.29 mmol based on the amount of In precursor used). The calculated yields reach >100%, which is due to the assumptions in the calculation of [InP], and has previously been well reported.[6,8]

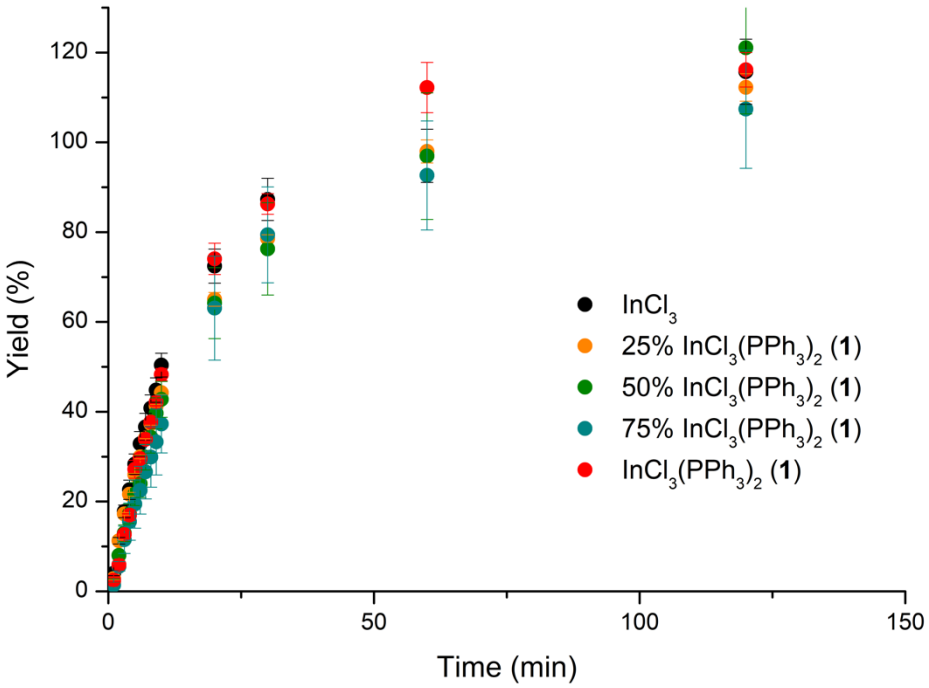

Figure S28. InP yield obtained using $InCl_3$ and ratios of **1.**

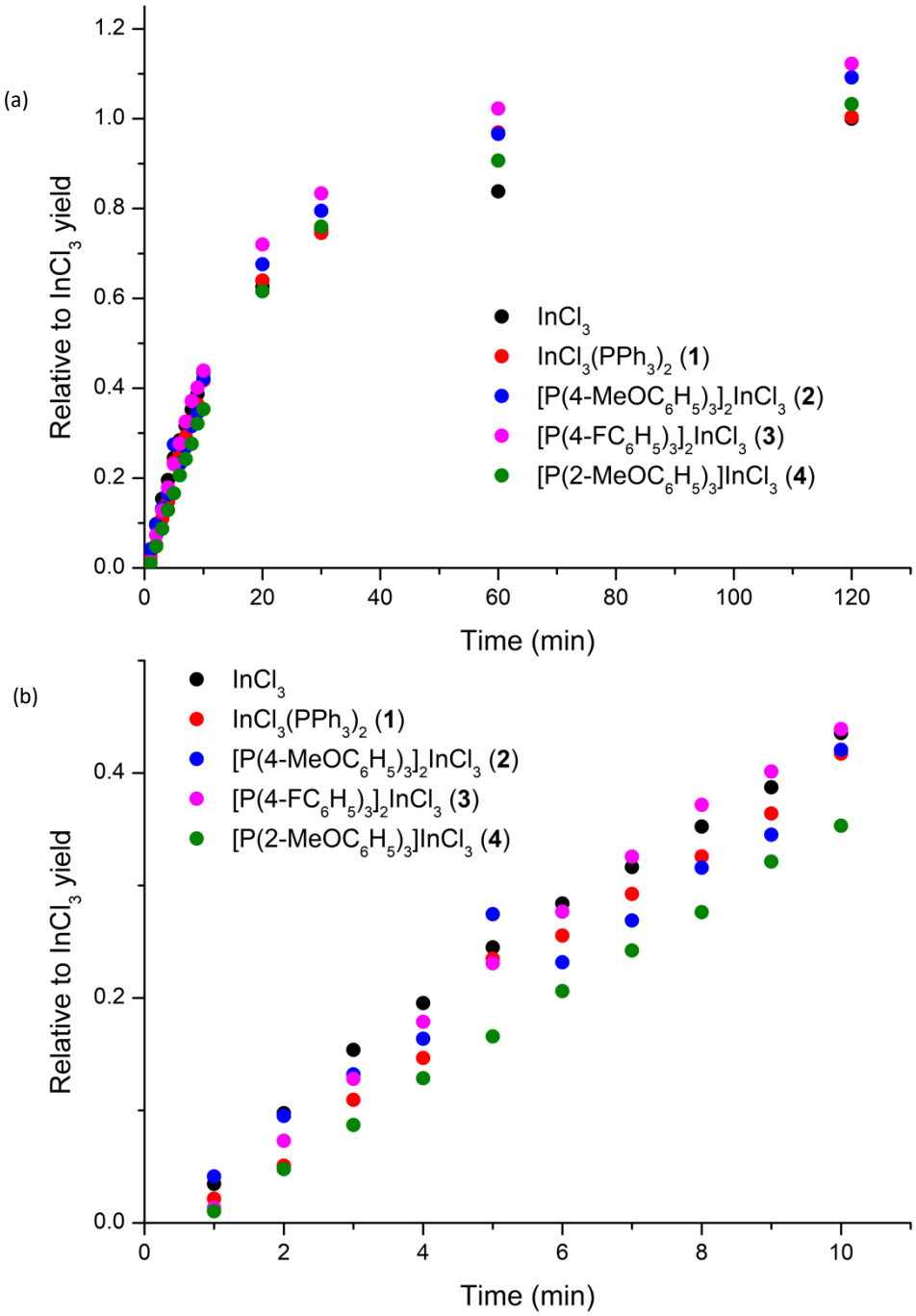

Figure S29. InP yield obtained using precursors **1**-**4** normalised to $InCl_3$ yield of 1.0 at 120 mins (a) over the whole reaction and (b) for the first 10 mins.

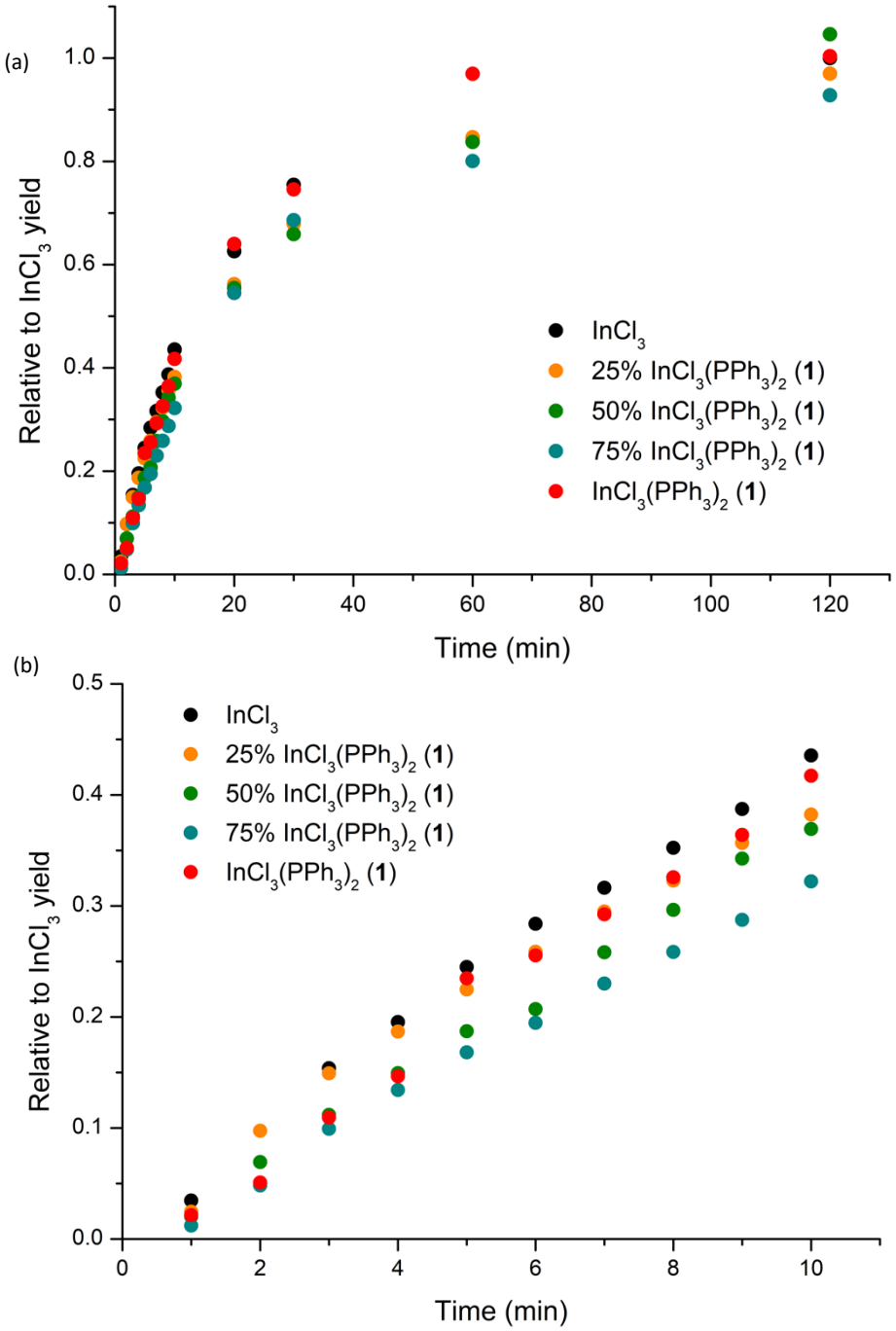

Figure S30. InP yield obtained using ratios of **1** : $InCl_3$ normalised to $InCl_3$ yield of 1.0 at 120 mins (a) over the whole reaction and (b) for the first 10 mins.

7. TEM Images

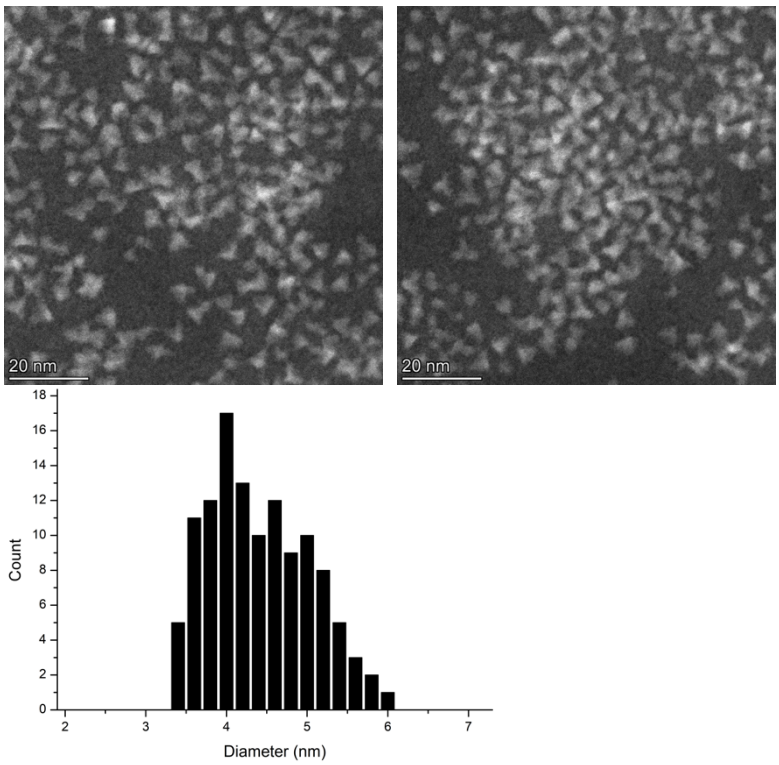

Figure S31. HAADF STEM images of InP QDs prepared from $InCl_3$ as the indium source. Sizes reported by measuring one length of a tetrahedron.

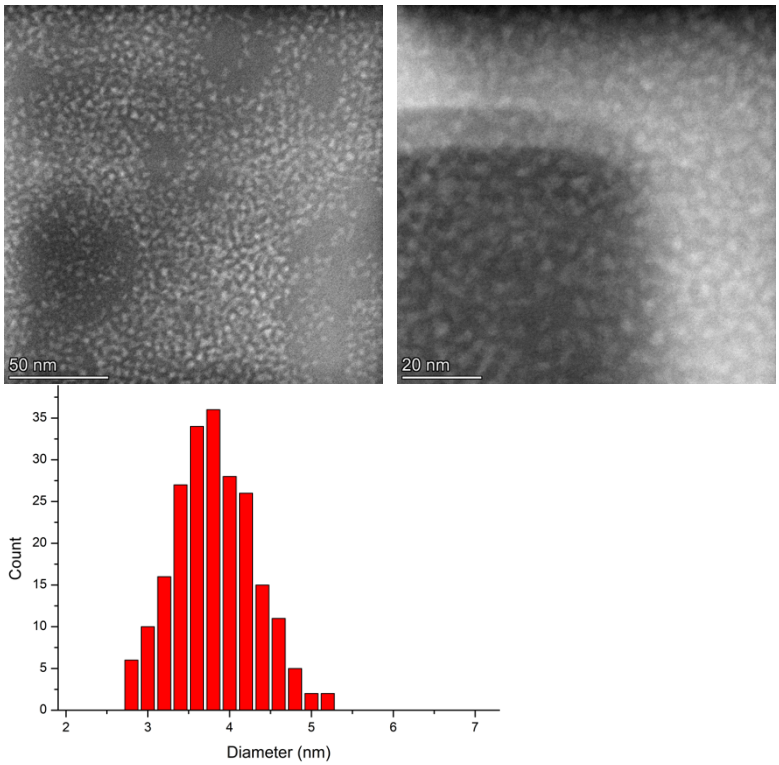

Figure S32. HAADF STEM images of InP QDs prepared from **1** as the indium source. Sizes reported by measuring one length of a tetrahedron.

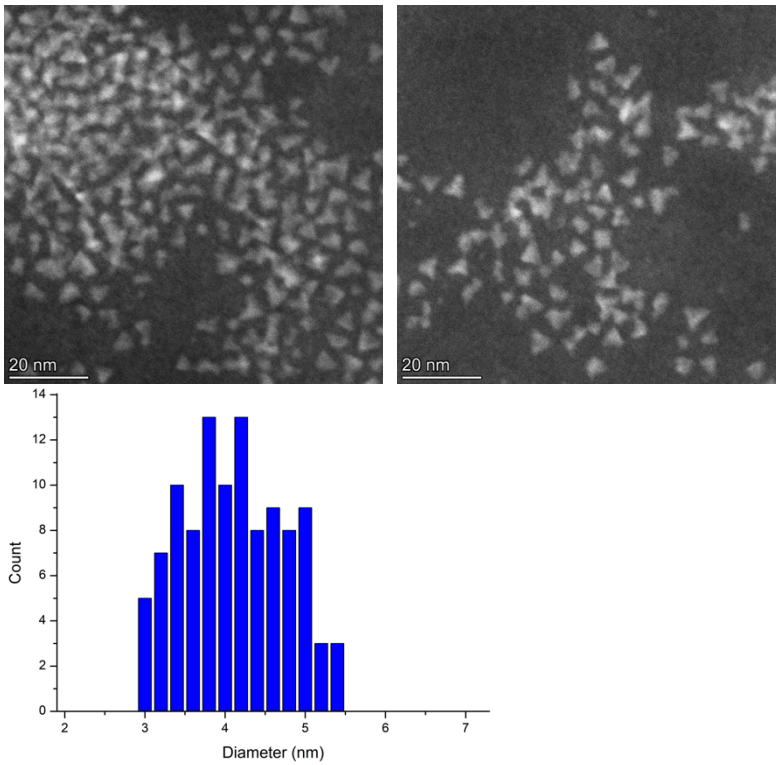

Figure S33. HAADF STEM images of InP QDs prepared from **2** as the indium source. Sizes reported by measuring one length of a tetrahedron.

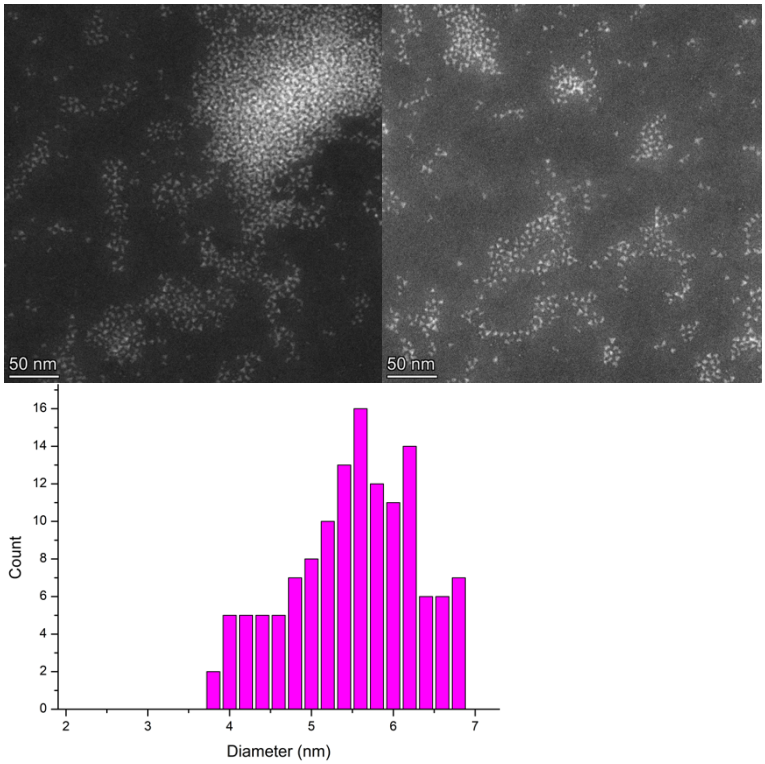

Figure S34. HAADF STEM images of InP QDs prepared from **3** as the indium source. Sizes reported by measuring one length of a tetrahedron.

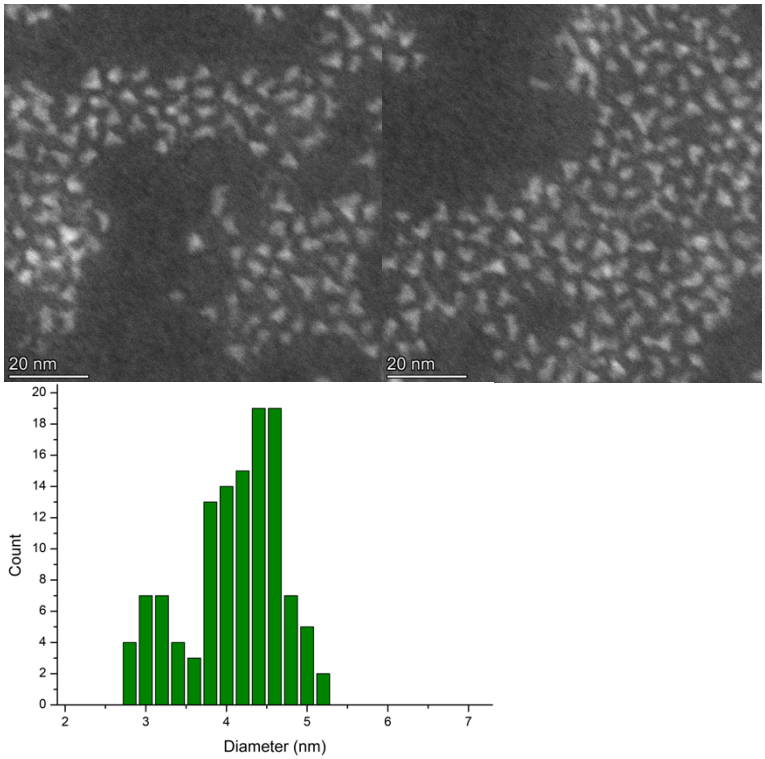

Figure S35. HAADF STEM images of InP QDs prepared from **4** as the indium source. Sizes reported by measuring one length of a tetrahedron.

8. XPS Spectra

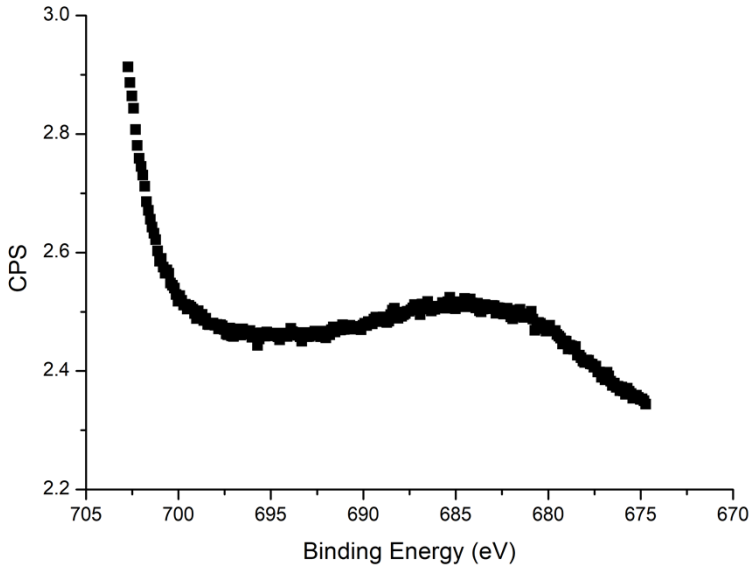

Figures S36. F 1S spectra of a purified sample of InP QDs prepared from **3**, showing no inclusion of F.

9. SANS/SAXS Data

Small-angle neutron scattering (SANS) measurements were carried out on the SANS2D beamline at the ISIS Neutron and Muon source, Rutherford Appleton Laboratory, UK. InP QD samples formed from all five precursors listed in Table 1 were studied. In all cases, InP QD samples were prepared in toluene-d8 to allow contrast between the deuterated solvent and ^{1}H-rich stabilising oleylamine ligand. Additionally, for the $InCl_3$ and $[P(2\text{-}MeOC_6H_4)_3]InCl_3$ precursors, contrast variation SANS (CV-SANS) measurements were performed on InP QDs in (i) toluene-h8 and in h:d toluene mixtures with ratios of (ii) 25:75 and (iii) 80:20. Samples were measured in 1 or 2 mm pathlength straight cells depending on 1H content, with the toluene-h8 and 80:20 h:d samples measured in 1 mm and the remainder being measured in 2 mm cells. A thermostatted sample changer provided temperature control. An 8 mm beam and two offset detectors with sample-to-detector distances of 2.36 and 4.00 m respectively were used, providing a detectable *Q* range of 0.005 – 0.9 $Å^{-1}$ for the merged datasets. Measurement times ranged from 30 min to 2 h depending on contrast, with the higher %H samples requiring longer runtimes to attain analyzable datasets. Raw data were radially averaged and corrected for transmission, background and detector efficiency using Mantid.[9,10] Data were placed on an absolute scale (cm^{-1}) using the scattering from a standard sample (a solid blend of hydrogenous and perdeuterated polystyrene).

Small-angle X-ray scattering measurements were performed using a 30W Cu microfocus sealed tube Xenocs Nano-inXider in the Materials Characterisation Lab at the ISIS Neutron and Muon source, Rutherford Appleton Laboratory, UK. The detectable *Q* range was 0.007 – 0.36 $Å^{-1}$ The same samples as to be measured using SANS in toluene-d8 were loaded into capillaries (in practice, a small amount was set aside for this purpose once the samples were made) and sealed using a glue gun. Multiple exposures of 2400 s for each sample were collected and averaged, giving final statistics equivalent to a single count time of just under 4 hr. Raw data were radially averaged and corrected for background (a toluene-d8 sample prepared in the same manner) using the Xenocs software. SAXS data was able to be collected on all precursors with the exception of $[P(4\text{-}FC_6H_4)_3]_2InCl_3$.

The corresponding SANS and SAXS data for the $(PPh_3)_2InCl_3$ and $[P(2\text{-}MeOC_6H_4)_3]InCl_3$ precursors is shown in Figure 4 in the main paper and for the remainder of the precursors is shown in Figure S8.1 below.

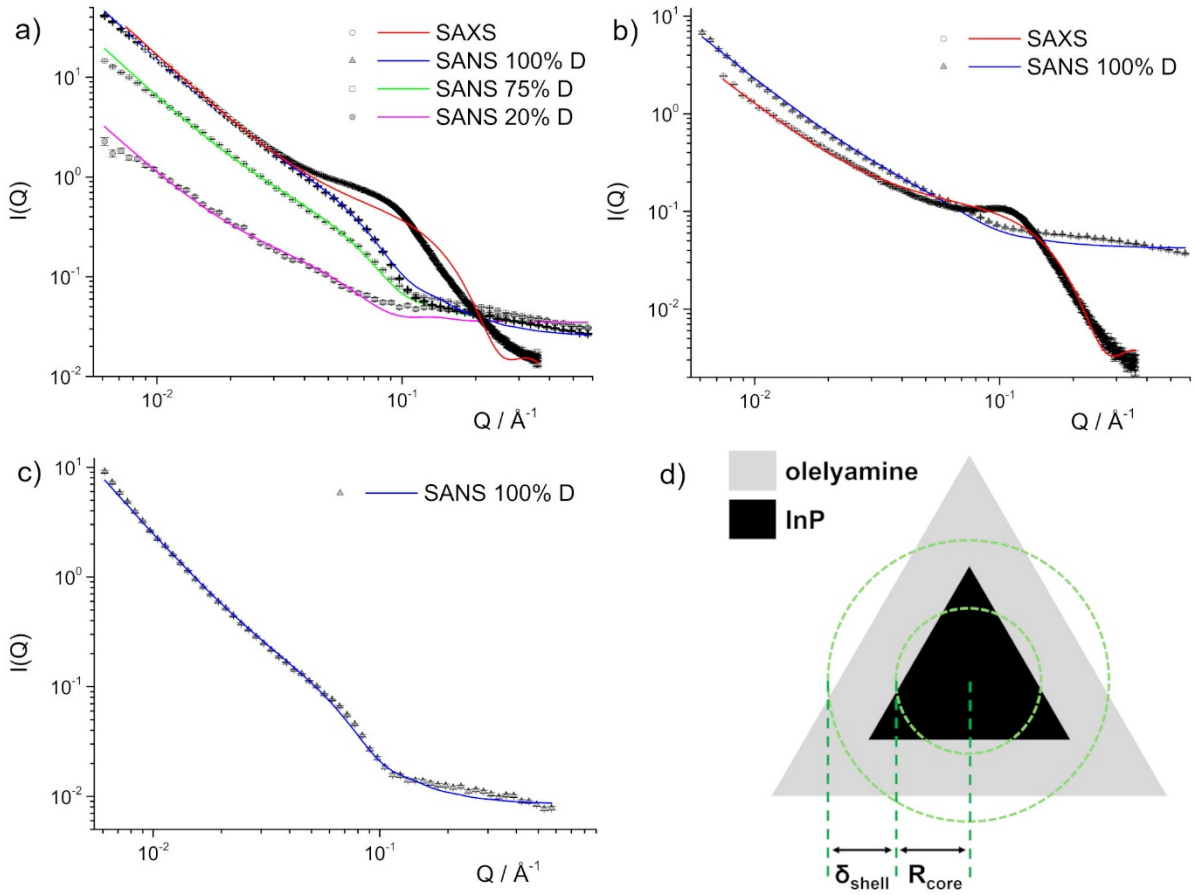

Figure S37. SANS and SAXS data for InP QDs formed with(a) $InCl_3$, (b) $[P(4\text{-}MeOC_6H_4)_3]InCl_3$ and (c) $[P(4\text{-}FC_6H_4)_3]_2InCl_3$ precursors. Lines are model fits to the data using a method as outlined in the text. In panel (a), contrast-variation SANS data was collected in mixtures of toluene-d8 and toluene-h8. In all cases, he "% D" in the legend indicates the %vol of toluene-d8 in that mixture. (d) Schematic depiction of how the core-shell sphere model may apply to the InP QD tetrahedron structure, accounting for rotation during the SANS measurement.

9.1 SAS analysis approach

All datasets were analyzed using a model representing a delta distribution of core-shell spheres to represent the InP QDs, with an additional power law and flat background to represent scattering contributions from loosely aggregated QDs and incoherent scattering from predominantly hydrogen atoms in the samples. The scattered intensity is then calculated using Equations S1 and S2.[7] In the equations below, "*scale*" is the volume fraction of scattering objects, ρ_i is the scattering length density of the parts *i* of the scattering system as noted, R_{core} is the spherical core radius, δ_{shell} the shell width and V_{core} and V_{total} the volume of the InP QD core and core+shell respectively.

$$I_{(q)} = \frac{scale}{V_{total}} F^2(Q) + aQ^b + I_{bkg} \quad \#(S1)$$

$$F(Q) = 3\left[(\rho_{core} - \rho_{shell})V_{core}\frac{\sin(Qr_{core}) - QR_{core}\cos(QR_{core})}{(QR_{core})^3} + (\rho_{shell} - \rho_{solvent})V_{tota}\right. \quad (S2)$$

In all cases except the $[P(4\text{-}FC_6H_4)_3]_2InCl_3$ precursor (for which only SANS in toluene-d8 was available for analysis), SAXS and SANS / CV-SANS datasets for each were analysed in SasView using a simultaneous globally constrained approach. Analysis was initially performed on the $InCl_3$ and $[P(2\text{-}MeOC_6H_4)_3]InCl_3$ precursor samples given the extra SAS data available for these. As noted in the MS, given the InP QDs were observed by microscopy to have an approximately tetrahedral shape, the use of a spherical model to analyse the SAS data is an approximation, albeit a reasonable one given rotation of the structure during SANS measurements. Here it is likely that the core-shell sphere describes the centre of the tetrahedron, as depicted above in Figure S37(d). For all datasets, δ_{shell} was fixed at 24 Å, which is the approximate extended length of the C_{18} alkyl chain in oleylamine, obtained using Tanford's formula ($l_c = 1.5 + 1.265\ n_c$ where n_c is the number of carbons in the alkyl chain). Scattering length densities, ρ_i were as follows: ρ_{core} was calculated as SANS = 1.8×10^{-6} Å^{-2} and SAXS = 35.8×10^{-6} Å^{-2} using the in-built calculator in SasView and a density of 4.8 g mL^{-1}. Likewise, $\rho_{solvent}$ for toluene-d8 was calculated as SANS = 5.66×10^{-6} Å^{-2} and SAXS = 8.0×10^{-6} Å^{-2}. For toluene-h8 this becomes SANS = 0.94×10^{-6} Å^{-2} (noting SAXS ρ is unaffected by deuteration). The SANS $\rho_{solvent}$ for h:d mixtures was calculated using proportional combinations of the above values.

For the CV-SANS samples ($InCl_3$ and $[P(2\text{-}MeOC_6H_4)_3]InCl_3$), analysis proceeded with the above values held constant and with globally constrained R_{core} and power law exponent, b. Here, ρ_{shell} was allowed to float within the range of $\rho_{shell,calc}$ (SANS: -0.17×10^{-6} Å^{-2}, SAXS: 7.8×10^{-6} Å^{-2}) and $\rho_{solvent}$. In both cases, for the sample in toluene-d8, a value of $\rho_{shell} = 3.2 \pm 0.2 \times 10^{-6}$ Å^{-2} was found, which points to solvent penetration into the oleylamine shell on the order of ~60%. In the analysis of the remaining datasets for the $[P(4\text{-}MeOC_6H_4)_3]InCl_3$, $(PPH_3)_2InCl_3$ and $[P(4\text{-}FC_6H_4)_3]_2InCl_3$ precursors, ρ_{shell} fixed as SANS = 3.2×10^{-6} Å^{-2} and SAXS = 3.2×10^{-6} Å^{-2} As above, R_{core} and power law exponent, b were globally constrained. Finally, in the case of $[P(4\text{-}FC_6H_4)_3]_2InCl_3$ precursor R_{core} was fixed at 1.7 nm given the SANS data quality and lack of SAXS data.

10. References

1 F. Chen, G. Ma, G. M. Bernard, R. G. Cavell, R. McDonald, M. J. Ferguson and R. E. Wasylishen, *J. Am. Chem. Soc.*, 2010, **132**, 5479–5493.

2 T. Allman and R. G. Goel, *Can. J. Chem.*, 1982, **60**, 716–722.

3 J. A. Bilbrey, A. H. Kazez, J. Locklin and W. D. Allen, *Journal of Computational Chemistry*, 2013, **34**, 1189–1197.

4 A. Haaland, A. Hammel, K.-G. Martinsen, J. Tremmel and H. V. Volden, *J. Chem. Soc., Dalton Trans.*, 1992, 2209.

5 D. C. Gary and B. M. Cossairt, *Chem. Mater.*, 2013, **25**, 2463–2469.

6 H. Larson and B. M. Cossairt, *Chem. Mater.*, 2023, **35**, 6152–6160.

7 M. D. Tessier, D. Dupont, K. De Nolf, J. De Roo and Z. Hens, *Chem. Mater.*, 2015, **27**, 4893–4898.

8 B. M. McMurtry, K. Qian, J. K. Teglasi, A. K. Swarnakar and J. De Roo, *Chem. Mater.*, 2020, **32**, 4358−4368.

9 R. Applin, R. Baust, A. Diaz-Alvarez, C. Finn, S. Foxley, J. Haigh, T. Hampson and P. F. Peterson, Mantid 6.9.1 (version 6.9.1) Mantid Project 2024.

10 O. Arnold, J. C. Bilheux, J. M. Borreguero, A. Buts, S. I. Campbell, L. Chapon, M. Doucet, N. Draper, R. Ferraz Leal, M. A. Gigg, V. E. Lynch, A. Markvardsen, D. J. Mikkelson, R. L. Mikkelson, R. Miller, K. Palmen, P. Parker, G. Passos, T. G. Perring, P. F. Peterson, S. Ren, M. A. Reuter, A. T. Savici, J. W. Taylor, R. J. Taylor, R. Tolchenov, W. Zhou and J. Zikovsky, *Nuclear Instruments and Methods in Physics Research Section A: Accelerators, Spectrometers, Detectors and Associated Equipment*, 2014, **764**, 156–166.